Random-anisotropy ferromagnetic state in the $Cu_5Gd_{0.54}Ca_{0.42}$ intermetallic compound

M. Krnel,[1] S. Vrtnik,[1] P. Koželj,[1] A. Kocjan,[1] Z. Jagličić,[2] P. Boulet,[3] M. C. de Weerd,[3] J. M. Dubois,[3] and J. Dolinšek[1,*]

[1]*J. Stefan Institute & University of Ljubljana, Faculty of Mathematics and Physics, Jamova 39, SI-1000 Ljubljana, Slovenia*

[2]*Institute of Mathematics, Physics and Mechanics & University of Ljubljana, Faculty of Civil and Geodetic Engineering, Jadranska 19, SI-1000 Ljubljana, Slovenia*

[3]*Institut Jean Lamour, Unités mixtes de recherche (UMR) 7198, Centre national de la recherche scientifique (CNRS) – Université de Lorraine, Parc de Saurupt, F-54011 Nancy, France*

(Received 21 December 2015; revised manuscript received 16 February 2016; published 11 March 2016)

By applying the alloy design concept that stable intermetallic phases between two immiscible elements can be formed by adding a third element that forms stable compounds with both elements, we have synthesized the first known stable intermetallic compound of Cu, Gd, and Ca, where copper acts as the mediating element between the immiscible Gd and Ca. A compound with the composition $Cu_{84}Gd_9Ca_7$ (equivalent to $Cu_5Gd_{0.54}Ca_{0.42}$) was synthesized by the Czochralski technique in the form of a large single crystal of high structural perfection, and the structural model was determined by x-ray diffraction (XRD). The compound crystallizes in the hexagonal system, space group $P6/mmm$, and the crystal structure is isotypic to the $Cu_{5.44}Tb_{0.78}$. The unit cell contains inherent disorder due to partial occupation of the Cu3 site and the substitutional disorder at the Gd/Ca mixed site located at the vertices of the hexagonal unit cell, where Gd and Ca randomly substitute each other. The random substitution of magnetic Gd by nonmagnetic Ca atoms makes the magnetic Gd lattice disordered, which leads to interesting magnetic ordering at low temperatures that occurs below $T_C = 24$ K in zero and low external magnetic fields. By performing a large set of complementary experiments along two perpendicular crystallographic directions (the [001] hexagonal-axis direction and the [100] hexagonal-plane direction), we show that the zero-field collective magnetic state can be described as a random-anisotropy ferromagnetic state, where random magnetic anisotropies originate from the magnetic dipole interactions between the Gd moments in the magnetically disordered lattice. The random-anisotropy ferromagnetic state in the $Cu_{84}Gd_9Ca_7$ is characterized by randomness and frustration of magnetic interactions, which are the two ingredients that allow classifying this state into the generic class of spin glasses. Our paper opens the possibility to search for new ternary intermetallic phases in the Cu–Gd–Ca phase diagram, including structurally complex phases and quasicrystals.

DOI: 10.1103/PhysRevB.93.094202

I. INTRODUCTION

Because of a 100% miscibility gap, the elements Ca and Gd do not form any stable compound, nor a solid solution, and there is no phase diagram available for the Ca–Gd system [1]. When a third element is added to two immiscible elements, the one that forms stable phases with both elements, new ternary intermetallic phases may form, and it is likely that some of these phases will have complex structure, either translationally periodic with a large unit cell or aperiodic but long-range ordered like quasicrystals and incommensurate phases. An example is the Al–Cu–Fe system, where copper and iron are completely immiscible, whereas aluminum reacts with both elements individually. In the Al–Cu–Fe ternary phase diagram, many intermetallic compounds, including icosahedral quasicrystals, are formed [2]. Other examples are the immiscible Cu and Ta, which both react with Al and form a bundle of complex intermetallic phases. The Al–Cu–Ta phase diagram comprises the $cF(23256\text{-}122)Al_{55.4}Cu_{5.4}Ta_{39.2}$ phase of unprecedented structural complexity, containing more than 23 000 atoms in the cubic unit cell [3]. For the Ca and Gd, a convenient third element to produce intermetallic phases is copper. Since Ca and Gd repel each other, it is intuitive to search for ternary compounds in the part of the Cu–Gd–Ca phase diagram with high concentration of the mediating element, hence in the Cu-rich corner. In the Cu–Ca binary phase diagram [4,5], there exists one Cu-rich intermetallic phase, namely Cu_5Ca, with hexagonal structure (space group $P6/mmm$, unit cell parameters $a = 5.074$ Å and $c = 4.074$ Å). The Cu–Gd phase diagram contains more Cu-rich phases [6–11]. These include Cu_7Gd, stable only at high temperatures (between about 690 and 840 °C), Cu_6Gd, Cu_5Gd, Cu_9Gd_2, and Cu_2Gd. The Cu_5Gd phase appears in two modifications: the low-temperature cubic $F\bar{4}3m$ with $a = 7.06$ Å, stable at room temperature, and the high-temperature hexagonal $P6/mmm$ with $a = 5.039$ Å and $c = 4.111$ Å, stable between 660 and 925 °C. According to the literature report [7], the Cu_5Gd cubic phase could not be obtained as a single phase but instead contained small amounts of the hexagonal modification. The stoichiometrically equivalent phases are thus Cu_5Ca and Cu_5Gd, which suggests searching for the Cu–Gd–Ca ternary phases along the $Cu_5Gd_{1-x}Ca_x$ composition line. Here we present successful synthesis of large single crystals of high structural perfection for the $x \approx 0.5$ composition. We have determined the structural model and measured anisotropic physical properties along different crystallographic directions. The compound shows complex magnetism that arises from random substitution of magnetic Gd by nonmagnetic Ca at a particular crystallographic site of the unit cell.

*Corresponding author: jani.dolinsek@ijs.si

II. SAMPLE PREPARATION AND STRUCTURAL MODEL

A large single crystal of centimeter dimensions was prepared by the Czochralski technique. The details on the crystal synthesis, characterization, and structure determination are given in the Supplemental Material (a photograph of the crystal is shown in Fig. S1) [12]. The samples for physical-property measurements were cut from the top part, where the energy-dispersive x-ray spectroscopy (EDS)-determined composition (in at. %) rounded to first integers was $Cu_{84}Gd_9Ca_7$ (equivalent to $Cu_5Gd_{0.54}Ca_{0.42}$). Since the crystal structure is hexagonal, we have cut from the parent crystal the samples along two different orthogonal crystallographic directions, one with the long dimension along the hexagonal axis (the [001] direction) and the other with the long dimension in the hexagonal plane (the [100] direction). For the measurements of the electrical and thermal conductivity and the thermoelectric power, the samples were rectangular rods of the size $7 \times 2 \times 2\,\mathrm{mm}^3$, whereas for the magnetic measurements we prepared small needles so that the SQUID detector was not saturated by the strong magnetic signal. Hall coefficient was determined on a plate of $10 \times 4 \times 1\,\mathrm{mm}^3$ dimensions, whereas the specific heat measurements were performed on a cube of 2 mm edge.

The x-ray diffraction (XRD) powder pattern (Fig. S2 of the Supplemental Material [12]) reveals sharp peaks that are characteristic of a crystalline material with good structural order. All peaks could be indexed to a hexagonal unit cell, space group $P6/mmm$, with the lattice parameters $a = 5.0591(2)$ Å and $c = 4.0919(2)$ Å. Atomic coordinates are given in Table 3 of the Supplemental Material [12], and the unit cell for the stoichiometric composition $Cu_5Gd_{0.5}Ca_{0.5}$ is shown in Fig. 1. The crystal structure is isotypic to the $Cu_{5.44}Tb_{0.78}$ type [8] and not to the Cu_5Ca type [4,5]. Actually this type corresponds to the Cu_5Ca type + one supplementary atomic position in $2e$ (0, 0, z), which is partially occupied by Cu atoms. Gd1 and Ca1 atoms occupy the mixed site $1a$ (0, 0, 0) located at the vertices of the hexagonal cell, where they randomly substitute each other. The average Gd and Ca occupancies depend on the actual composition of the crystal. Since the composition of the crystal used for our measurements was off-stoichiometric ($Cu_5Gd_{0.54}Ca_{0.42}$), the mixed site is slightly Gd rich. Cu1 atoms are located in the center of the unit cell and in the centers of the side planes. Cu2 atoms are located in the base plane, each one in the center of a triangle formed by the three neighboring Gd/Ca atoms. Cu3 atoms are located at the edges parallel to the 6-axis, occupying the supplementary $2e$ (0, 0, z) position, and the occupation is partial and rather low (about 6%). The structure thus contains inherent disorder due to the substitutional disorder at the Gd/Ca site and the partial occupation of the Cu3 site.

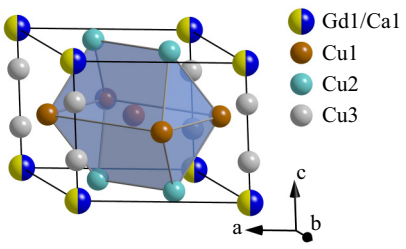

FIG. 1. The hexagonal unit cell of $Cu_5Gd_{0.5}Ca_{0.5}$.

III. RESULTS

Magnetic measurements were conducted by a Quantum Design MPMS XL-5 SQUID magnetometer equipped with a 5 T magnet. Electrical and thermal transport properties (electrical resistivity, magnetoresistance, thermoelectric power, Hall coefficient, thermal conductivity) and the specific heat were measured by a Quantum Design Physical Property Measurement System (PPMS) 9T.

A. Magnetic measurements

The $Cu_{84}Gd_9Ca_7$ single crystal shows anisotropy of magnetic properties between the hexagonal-axis direction and the hexagonal plane. To determine this anisotropy, we have performed two sets of identical experiments: one for the magnetic field along the [001] hexagonal-axis direction and the other for the field in the hexagonal plane (the [100] direction).

1. Temperature-dependent magnetization

(a) Magnetic field along the [001] hexagonal-axis direction. The temperature-dependent zero-field-cooled (zfc) magnetization M_{zfc} and the field-cooled (fc) magnetization M_{fc} at temperatures below 40 K in magnetic fields between 0.5 mT and 0.8 T are shown in Fig. 2(a). In the lowest investigated magnetic field of $B = 0.5$ mT, a sharp transition to a collective magnetic state is observed at $T_C = 24$ K. Both M_{zfc} and M_{fc} are small in this field and exhibit different temperature dependence for different thermal histories. This is shown in the inset of Fig. 2(a), where the measurements for three different protocols (fc measurement on cooling, fc measurement on heating, and zfc measurement on heating) are presented on an expanded scale. It is evident that each protocol yields a different $M(T)$ curve below T_C. In increasing magnetic fields, M_{zfc} and M_{fc} grow strongly up to the field value of $B \approx 0.1$ T, whereas the $M_{\mathrm{zfc}} - M_{\mathrm{fc}}$ difference decreases. For fields higher than 0.1 T, the $M_{\mathrm{zfc}} - M_{\mathrm{fc}}$ difference has already vanished, and the magnetization at the lowest measured temperature of 2 K does not increase significantly with the magnetic field anymore. Inspecting the magnetization curves in the region of T_C, we notice that the growing external magnetic field smears the phase transition over an increasingly larger temperature interval. The shapes of the $M(T)$ curves resemble ferromagnetic (FM) curves with a field-induced smearing of the FM transition.

(b) Magnetic field in the hexagonal plane (along the [100] direction). The temperature-dependent M_{zfc} and M_{fc} curves in the same range of magnetic fields are presented in Fig. 2(b). The growth of M_{zfc} and M_{fc} with the magnetic field applied in the hexagonal plane is slower than for the hexagonal-axis direction and the 2 K magnetization values do not increase significantly anymore for fields $B > 0.4$ T. In the lowest investigated magnetic fields, M_{zfc} and M_{fc} exhibit a maximum at $T_C = 24$ K and then decrease slightly upon further cooling, resembling antiferromagnetic (AFM) curves. A tiny $M_{\mathrm{zfc}} - M_{\mathrm{fc}}$ splitting is also present. This is best observed in the

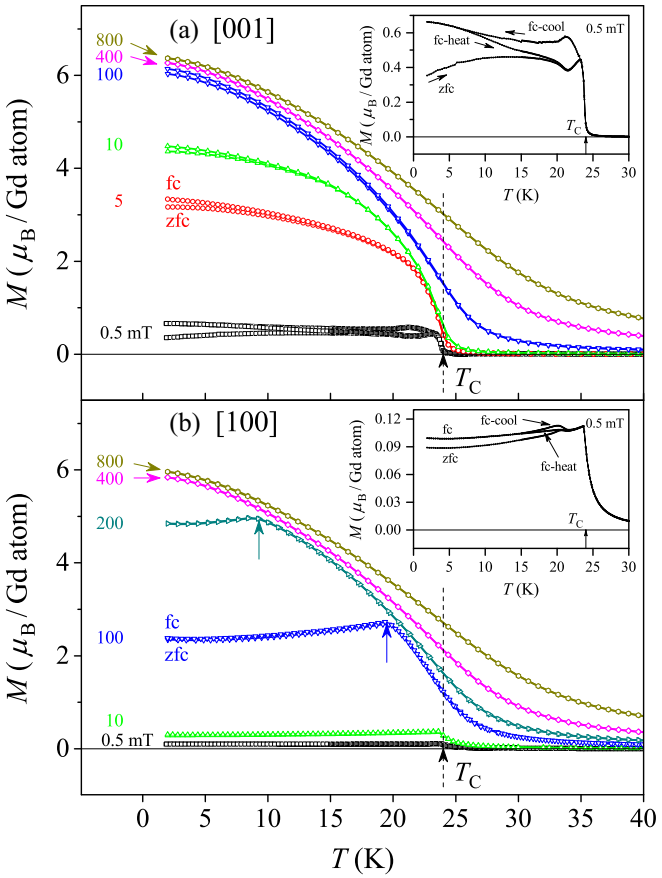

FIG. 2. Temperature-dependent zfc and fc magnetizations below 40 K in magnetic fields between 0.5 mT and 0.8 T for the magnetic field (a) along the [001] hexagonal-axis direction and (b) in the hexagonal plane (the [100] direction). Insets: M_{zfc} and M_{fc} in the lowest investigated magnetic field of $B = 0.5$ mT for different measurement protocols: fc measurement on cooling (fc-cool), fc measurement on heating (fc-heat), and zfc measurement on heating. The solid vertical arrows on the 100 mT and 200 mT curve in panel (b) mark the transition where the FM-type $M(T)$ dependence changes into the AFM-type.

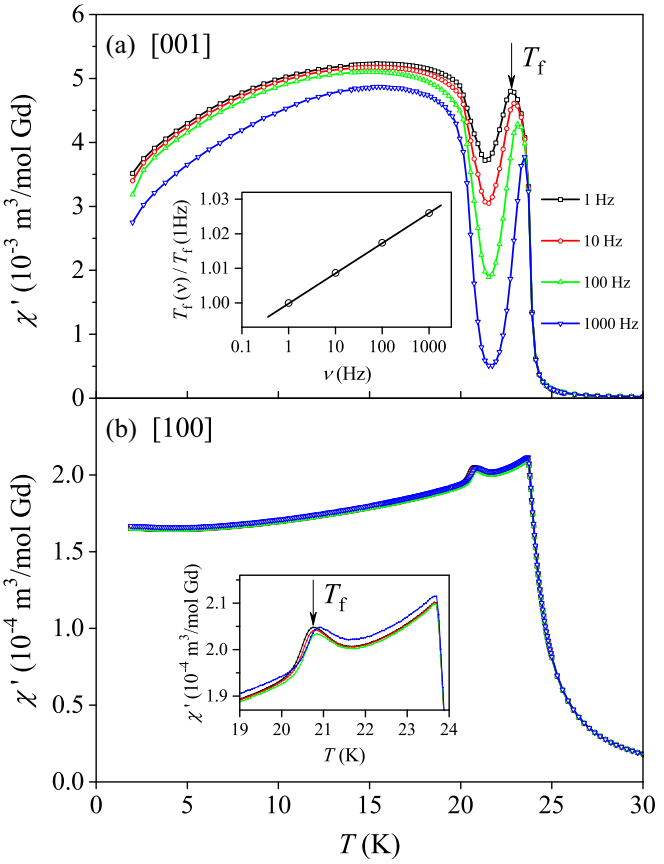

FIG. 3. Real part of the ac susceptibility χ' at temperatures below 30 K, measured at frequencies 1, 10, 100, and 1000 Hz for the magnetic field (a) along the [001] hexagonal-axis direction and (b) in the hexagonal plane (the [100] direction). (a) Inset: frequency dependence of the spin freezing temperature $T_f(\nu)$ (marked by an arrow on the 1 Hz curve) normalized to $T_f(1\text{ Hz})$. (b) Inset: expanded portion of χ' in the region of the phase transition at $T_C = 24$ K (the arrow on the 1 Hz curve marks the freezing temperature, as discussed in the text).

$B = 0.5$ mT curves, which are presented on an expanded scale in the inset of Fig. 2(b). The magnetization values in this field are considerably smaller (by a factor of about 5) than for the hexagonal-axis direction [inset in Fig. 2(a)], and the $M(T)$ shapes also depend on the measurement protocol (fc measurement on cooling, fc measurement on heating, and zfc measurement on heating), though in a different way than for the other field direction. Increasing magnetic field shifts the magnetization maximum from T_C to lower temperatures and the shift is accompanied by a qualitative change of the $M(T)$ shape from the AFM-type below the maximum to the FM-type above (the apparent AFM-to-FM transition temperature is marked by a solid vertical arrow on the 100 mT and 200 mT curves), where the magnetic field-induced smearing of the FM transition at $T_C = 24$ K is also evident. In the high-field region ($B > 0.4$ T), the magnetization curves for both field directions match, being entirely of the FM type. The anisotropy of the magnetization is thus manifest only in the low-field regime.

2. *Ac susceptibility*

Ac susceptibility measures the response of the spin system to an ac magnetic field. We have used a sinusoidal magnetic field of amplitude $B_0 = 0.65$ mT and frequencies $\nu = 1$, 10, 100, and 1000 Hz. Different behavior was found for the ac field along the hexagonal axis and in the hexagonal plane.

(a) Ac field along the [001] hexagonal-axis direction. The real part of the ac susceptibility χ' in the temperature range below 30 K is shown in Fig. 3(a), where two distinct features are observed. Upon crossing the phase transition, χ' first exhibits a sharp peak, which shifts to higher temperatures with increasing frequency of the ac field. Such behavior is found in dynamic spin systems with a distribution of motional correlation times, where spin fluctuations gradually slow down and freeze on the experimental time scale upon cooling. Examples are spin glasses and superparamagnets. The temperature where the peak reaches its maximum value can be associated with the frequency-dependent spin freezing temperature $T_f(\nu)$ [marked by an arrow on the 1 Hz curve in Fig. 3(a)]. The $T_f(\nu)$ relation

is shown in the inset of Fig. 3(a), where $T_f(\nu)$ normalized to $T_f(1\,\mathrm{Hz}) = 22.7\,\mathrm{K}$ is presented. A logarithmic dependence of T_f on the frequency is evident, and the freezing temperature at the highest measured frequency of 1 kHz has increased by a factor 1.03 to a value $T_f(1\,\mathrm{kHz}) = 23.3\,\mathrm{K}$. The fractional shift of the freezing temperature per decade of frequency was evaluated to be $\Gamma = \Delta T_f/T_f\Delta(\log\nu) = 0.0087$, which is considerably smaller than the Γ values typically found in spin glasses (e.g., canonical spin glasses like AuFe and PdMn are characterized by values in the range $\Gamma \approx$ 0.01–0.06) and are much smaller than in superparamagnets (where $\Gamma \approx 0.3$) [13]. The smallness of Γ indicates that the magnetic phase transition in $Cu_{84}Gd_9Ca_7$ is close to a thermodynamic phase transition (in which case the peak in the ac susceptibility should not shift with the frequency), but there is a narrow superparamagnetic regime in the vicinity of T_C where spins (or spin clusters) perform thermally assisted jumping between energetically similar states and gradually freeze below T_C.

The second distinct feature in χ' is a broad maximum that develops in the low-temperature region below 20 K. The maximum is so broad that it is difficult to judge whether it depends on the frequency. This broad maximum indicates the presence of spin fluctuations, which exist down to the lowest investigated temperature of 2 K and the spectrum of motional correlation times is very broad, much broader than the one responsible for the freezing dynamics within the superparamagnetic regime in the vicinity of T_C. Spin fluctuations responsible for the appearance of the broad maximum below 20 K may be the elementary excitations of the collective magnetic state that develops below T_C.

(b) Ac field in the hexagonal plane (along the [100] direction). The real part of the ac susceptibility χ' for the ac field applied in the hexagonal plane [Fig. 3(b)] is one order of magnitude smaller than for the field along the hexagonal axis. χ' forms a frequency-independent maximum at $T_C = 24\,\mathrm{K}$, suggesting a thermodynamic phase transition. A small additional maximum is observed around $T \approx 21\,\mathrm{K}$, which depends weakly on the frequency [inset in Fig. 3(b)]. Associating the peak temperature of this additional maximum with the freezing temperature $T_f(\nu)$ (marked by an arrow on the 1 Hz curve in the inset), we find $T_f(1\,\mathrm{Hz}) = 20.75\,\mathrm{K}$ and $T_f(1\,\mathrm{kHz}) = 20.92\,\mathrm{K}$ with a very small increase factor of 1.008. The fractional shift of T_f per decade of frequency was evaluated to be $\Gamma = 0.0027$. This Γ value is so small that it cannot represent a spin-freezing transition in the sense of spin glasses and superparamagnets, though some spin entities still freeze upon cooling. The above results suggest that the spins system is considerably stiffer, and the spin clusters are less reorientable by the external magnetic force when the ac field is applied in the hexagonal plane, as compared to the field along the hexagonal-axis direction.

3. *Paramagnetic susceptibility*

Magnetic susceptibility $\chi = M/H$ in a magnetic field $\mu_0 H = 0.1\,\mathrm{T}$ applied along the [100] hexagonal-plane direction in the entire investigated temperature range up to 300 K is shown in Fig. 4 in a χ^{-1} versus T plot. Within the paramagnetic regime (at $T > T_C$), the $\chi(T)$ relation can be described by the

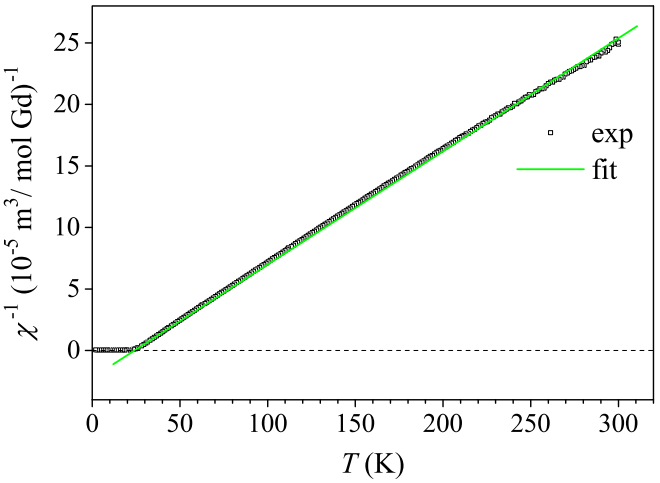

FIG. 4. Magnetic susceptibility $\chi = M/H$ in a magnetic field $\mu_0 H = 0.1\,\mathrm{T}$ applied along the [100] hexagonal-plane direction in the entire investigated temperature range up to 300 K in a χ^{-1} versus T plot. Solid line is the fit of the paramagnetic susceptibility with the Curie-Weiss law.

Curie-Weiss law

$$\chi = \frac{C_{\mathrm{CW}}}{T - \theta}, \tag{1}$$

where C_{CW} is the Curie-Weiss constant and θ is the Curie-Weiss temperature. The constant C_{CW} gives information on the magnitude of the Gd moments, whereas the type and strength of the coupling between the moments can be estimated from the magnitude and sign of θ. There can be an additional temperature-independent term χ_0 added to the right side of Eq. (1), accounting for the Larmor diamagnetic contribution χ_{dia} due to the atomic cores and the two contributions from the conduction electrons—the Landau diamagnetic contribution χ_L due to the electron orbital circulation and the Pauli spin paramagnetic contribution χ_P. The Larmor susceptibility was calculated from literature tables to amount $\chi_{\mathrm{dia}} = -1.6 \times 10^{-8}\,\mathrm{m^3\,mol^{-1}}$. The Landau and Pauli contributions are of the same (absolute) order of magnitude as χ_{dia} so that the constant term χ_0 is much smaller than the Curie-Weiss susceptibility of the Gd atoms. For that reason χ_0, was omitted from Eq. (1).

The fit of the data for $T > 50\,\mathrm{K}$ (solid line in Fig. 4) yielded the parameter values $C_{\mathrm{CW}} = 1.07 \times 10^{-4}\,\mathrm{m^3\,K\,(mol\,Gd)^{-1}}$ and $\theta = 24.1\,\mathrm{K}$. The Curie-Weiss constant C_{CW} was used to determine the mean effective magnetic moment $\bar{\mu}_{\mathrm{eff}} = \bar{p}_{\mathrm{eff}}\mu_B$ per Gd ion. Here μ_B is the Bohr magneton, and $\bar{p}_{\mathrm{eff}}$ is the mean effective Bohr magneton number that can be calculated using the formula [14] $\bar{p}_{\mathrm{eff}} = \sqrt{3C_{\mathrm{CW}}k_B/(N_A\mu_B^2\mu_0)}$ (where N_A is the Avogadro number). We obtained $\bar{p}_{\mathrm{eff}} = 8.2 \pm 0.2$, which is within the experimental uncertainty equal to the measured Bohr magneton number of a bare Gd^{3+} ion ($p = 8.0$), demonstrating that the Gd magnetic moments in the $Cu_{84}Gd_9Ca_7$ assume their full free-ion values.

The spin-spin exchange coupling strength can be estimated from the Curie-Weiss temperature. The positive θ value demonstrates a FM-type parallel exchange coupling between the spins. At high temperatures ($\theta/T \ll 1$), the Curie-Weiss

law of Eq. (1) can be rewritten in the form of a modified Curie law $\chi \approx (C_{CW}/T)(1+\theta/T)$, where θ/T is the leading high-temperature correction factor originating from the exchange interaction between the spins. Using the Heisenberg spin Hamiltonian, one obtains $\theta = [S(S+1)/3](J_0/k_B)$, where S is the spin quantum number and $J_0 = \sum_{\vec{R}} J(\vec{R})$ is the sum of the exchange coupling constants of a given spin (located at the origin) to all neighboring spins in the lattice (located at the lattice points $\vec{R}$) [15]. Taking the spin of a Gd^{3+} ion $S = 7/2$ and $\theta = 24.1$ K, we obtain $J_0/k_B = 4.6$ K.

Since the magnetic moments of Gd^{3+} ions are sizable, it is instructive to estimate the strength of the magnetic dipole-dipole interaction between the nearest-neighbor Gd atoms. The shortest distance between two Gd atoms in the $Cu_{84}Gd_9Ca_7$ structure is one lattice parameter along the hexagonal-axis direction ($c \approx 4.1$ Å). The order of magnitude of the dipole-dipole energy for a nearest-neighbor pair of Gd moments is obtained as $E_{dd}/k_B \approx (\mu_0/4\pi)(\bar{p}_{eff}\mu_B)^2/c^3k_B = 0.6$ K. Though this energy is small compared to the exchange coupling energy, the dipolar coupling is a long-range interaction so that many dipolarly coupled spins may introduce significant magnetic anisotropy and be responsible for the anisotropic magnetism of the $Cu_{84}Gd_9Ca_7$.

4. Magnetization versus the magnetic field curves

The magnetic state of the $Cu_{84}Gd_9Ca_7$ crystal was further investigated by the magnetization $M(H)$ curves measured for the magnetic field sweep $\mu_0 H = \pm 5$ T. The $M(H)$ curves for a selected set of temperatures below 50 K are shown in Fig. 5(a) for the field along the [001] hexagonal-axis direction and in Fig. 5(b) for the field in the hexagonal plane (the [100] direction). For both directions, we observe that the increase of magnetization with the field towards a saturated value is faster at lower temperatures, and the 5 K magnetization in the highest field of 5 T reaches the value of 6.7 μ_B/Gd atom. The theoretical saturated magnetization in the $T \to 0$ limit [marked by a dashed line in Figs. 5(a) and 5(b)] is $M_s = gJ\mu_B$, where $g = 2$ is the Landé factor and $J = 7/2$ is the total angular momentum of Gd^{3+}, yielding $M_s = 7\mu_B$. Since the experimental $M(H)$ curves still grow slightly with the field at 5 T (and also with the decreasing temperature), it is likely that the experimental saturated magnetization for both field directions reaches the theoretical value at higher fields

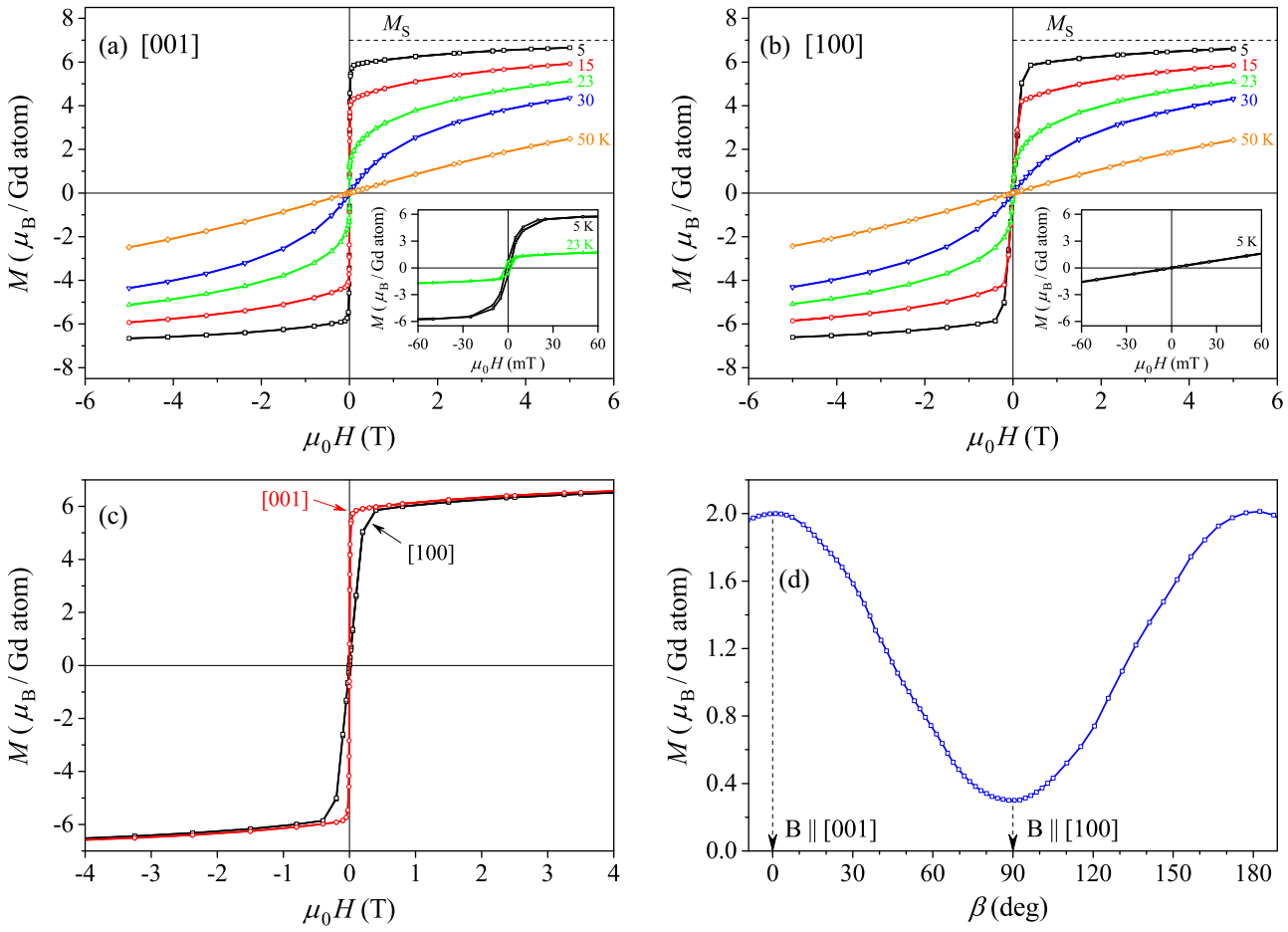

FIG. 5. $M(H)$ curves below 50 K for the field (a) along the [001] hexagonal-axis direction and (b) in the hexagonal plane (the [100] direction). Dashed line marks the theoretical saturated magnetization $M_s = 7\mu_B$ in the $T \to 0$ limit. Insets: $M(H)$ hysteresis loops at $T < T_C$ on an expanded scale. (c) Comparison of the $M(H)$ curves at $T = 5$ K for the two investigated magnetic-field directions. (d) Angular dependence of the magnetization for rotation about an axis lying in the hexagonal plane, performed at $T = 20$ K in the field $B = 10$ mT. The angle $\beta = 0$ corresponds to the orientation where the field is parallel to the hexagonal axis.

and lower temperatures so that no spins are lost in the total saturated magnetization and all Gd moments in the structure are polarized along the field direction.

The $M(H)$ curves for the two investigated field directions show the anisotropy, which is best seen by comparing the two 5 K curves [Fig. 5(c)]. For the hexagonal-axis direction, the field as small as 20 mT is already enough to almost completely polarize the Gd spins along the field at that temperature [this field value corresponds to the point where the initial strong $M(H)$ dependence turns into a weak one and the magnetization reaches about 90% of the saturated value]. For the field in the hexagonal plane, a significantly larger field of 400 mT is needed to achieve the same polarization. The robustness of the magnetization anisotropy in the low-field regime is also evident from the angular dependence of the magnetization for rotation about an axis lying in the hexagonal plane. The experiment [Fig. 5(d)] was performed at the temperature $T = 20$ K in the field $B = 10$ mT. It is seen that the magnetization anisotropy (where the magnetization is larger for the field along the hexagonal-axis direction) is reversibly reproduced at this low field value upon rotating the crystal. From Fig. 5(c) it is, however, evident that the anisotropy is no longer present for the field larger than about 400 mT, as the external magnetic field is already strong enough to polarize the spins along the field direction and destroy the anisotropic magnetic structure that develops in zero (and low) magnetic fields below T_C.

Anisotropy is observed also in the width of the $M(H)$ hysteresis loops upon field cycling. The $M(H)$ curves for the field along the [001] hexagonal-axis direction are shown expanded around the origin in the inset of Fig. 5(a). Hysteresis is observed below T_C, but the hysteresis loops are narrow with the coercive field $\mu_0 H_c \approx 1.2$ mT, which does not change significantly with temperature. This coercive field value is small enough that it may be affected by the remanence of the superconducting magnet of the employed SQUID magnetometer, which is up to a few tenths of a mT. The field value at which the hysteresis loops close up amounts to about 20 mT, a value which is small even for a FM-type hysteresis (where the loops close up typically in a field of a few 100 mT). The $M(H)$ hysteresis curve at $T = 5$ K for the field in the hexagonal plane is shown in the inset of Fig. 5(b). For this field direction, the width of the hysteresis loops is so small that it cannot be distinguished from the remanence of the magnet so that the coercive field is close to zero, $\mu_0 H_c \approx 0$. The $Cu_{84}Gd_9Ca_7$ crystal thus shows tiny hysteresis for the field along the hexagonal-axis direction, whereas no hysteresis can be claimed beyond the experimental uncertainty for the field in the hexagonal plane.

5. *Thermoremanent magnetization*

Intrinsic disorder in the $Cu_{84}Gd_9Ca_7$ structure is expected to produce some degree of frustration of magnetic interactions (i.e., no spin configuration can satisfy all the bonds and minimize the energy at the same time). In magnetically frustrated systems, ergodicity of the spin system is generally broken at low temperatures. A system is called nonergodic if the correlation times for internal motions are longer than the observation time window of a given experimental technique so that the system cannot visit the complete phase space during the experiment. Within the nonergodic phase, thermal fluctuations are no more efficient to maintain thermal equilibrium on experimentally accessible time scales so that the experimental values of physical parameters become time-dependent, in contrast to ergodic systems where time-independent (thermodynamic) values are measured. The out-of-equilibrium dynamics of a nonergodic spin system are related to slow approach towards a thermodynamic equilibrium, which can globally never be reached due to macroscopic equilibration times. An experimental manifestation of broken ergodicity is a logarithmically slow time decay of the thermoremanent dc magnetization (TRM) [16,17]. In a TRM experiment, one cools the sample in a magnetic field B from the ergodic into the nonergodic phase, and the cooling is stopped at the measuring (and, at the same time, aging) temperature T_1, where the spin system is let to age for a waiting (aging) time t_w. After t_w, the field is suddenly cut to zero, and the magnetization time-decay is measured over macroscopic times. Upon $B \to 0$, the reversible part of the fc magnetization $M_{\rm fc}$ decays to zero almost instantaneously, whereas the irreversible part (the TRM) decays very slowly in time. The TRM is a fraction of $M_{\rm fc}$ prior to cutting the field to zero, and, depending on temperature, its magnitude amounts from a few percent up to almost full $M_{\rm fc}$. The TRM decay depends on the aging temperature T_1, the aging time t_w, and the field value B in which the aging is performed.

In our TRM-decay experiments, the crystal was cooled from room temperature to different measuring temperatures in the field $B = 5$ mT applied along the hexagonal-axis direction to different measuring temperatures, and the aging time of $t_w = 1$ h was employed in each case. The TRM decay was monitored for a time 120 min after the field switch off. The TRM decay curves normalized to the magnetization prior to cutting the field to zero, $M_{\rm TRM}(T_1,t)/M_{\rm fc}(T_1)$ for the stop temperatures $T_1 = 2$, and 20 K $< T_C$ are displayed in Fig. 6. The following observations are evident: (1) The TRM is

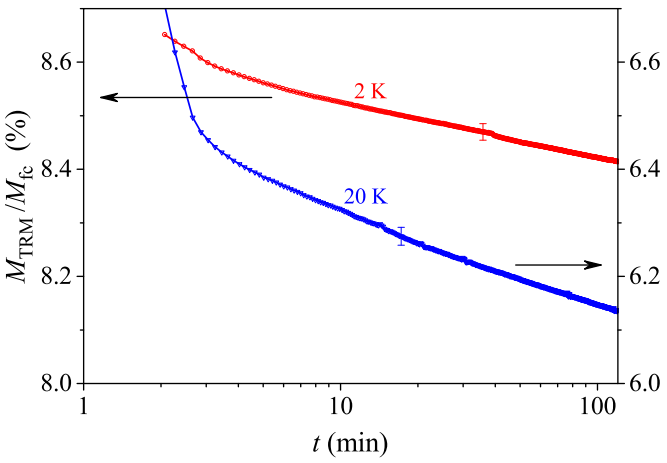

FIG. 6. The TRM time-decay curves normalized to the magnetization prior to cutting the field to zero, $M_{\rm TRM}(T_1,t)/M_{\rm fc}(T_1)$ for the stop temperatures $T_1 = 2$, and 20 K $< T_C$. Cooling and aging were performed in a field $B = 5$ mT applied along the hexagonal-axis direction, and the aging time $t_w = 1$ h was employed.

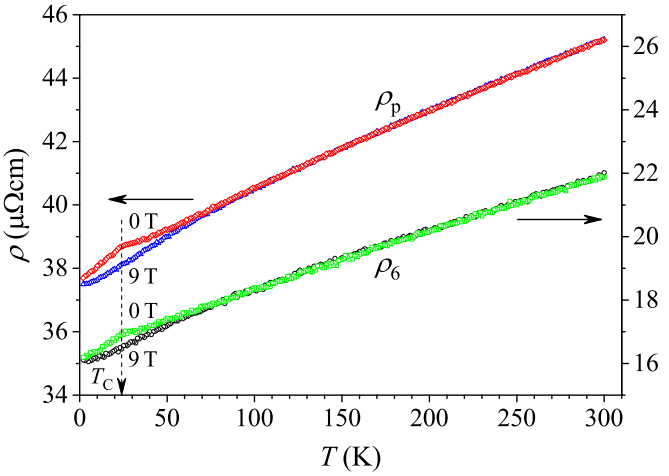

FIG. 7. Temperature-dependent electrical resistivity for the current along the hexagonal axis (ρ_6) and in the hexagonal plane (ρ_p) in magnetic fields 0 and 9 T. Dashed vertical line marks $T_C = 24$ K.

nonzero within the collective magnetic state, and its fraction in the total magnetization is larger at lower temperature, as a consequence of the increased remanence of the spin system upon cooling; (2) TRM decays are logarithmically slow in time t, the decay is slower at lower temperature, and the decay time constant changes with the time; and (3) within the investigated time interval of 120 min, the TRMs decay continuously, and it cannot be inferred to what kind of asymptotic value they approach in the $t \to \infty$ limit (either to a nonzero spontaneous magnetization or to a zero magnetization). This TRM behavior proves that the ergodicity of the spin system is broken on the experimental time scale, indicating that frustration is present in the collective magnetic state below T_C.

B. Electrical resistivity and magnetoresistance

Electrical resistivity in the temperature range between 2 and 300 K for the current along the [001] hexagonal-axis direction, denoted as ρ_6, and in the hexagonal plane (the [100] direction), denoted as ρ_p, in magnetic fields 0 and 9 T is shown in Fig. 7. There is a significant anisotropy between the two directions, with ρ_p being roughly a factor of 2 larger than ρ_6 in the entire investigated temperature range, so that the hexagonal-axis direction is the more conducting one. Both resistivities show positive temperature coefficient. For the hexagonal-axis direction, the residual resistivity amounts to $\rho_6^{2\,\mathrm{K}} = 16.2\ \mu\Omega$cm, and the room-temperature resistivity is $\rho_6^{300\,\mathrm{K}} = 22.0\ \mu\Omega$cm, whereas for the hexagonal-plane direction the resistivity values are $\rho_p^{2\,\mathrm{K}} = 37.5\ \mu\Omega$cm and $\rho_p^{300\,\mathrm{K}} = 45.0\ \mu\Omega$cm. Interesting behavior is observed when comparing the resistivities in zero magnetic field and in a 9 T field. For both crystallographic directions, the zero-field resistivity shows an enhancement with respect to the 9 T resistivity in the low-temperature region below about 70 K, and the enhancement reaches its maximum at the temperature 24 K, thus at T_C. The 9 T resistivity shows smooth monotonous increase with no anomaly upon heating in the entire investigated temperature range.

The resistivity in the temperature interval between 100 and 2 K, measured in magnetic fields between 0 and 9 T in steps of $\Delta B = 1$ T, is shown in Fig. 8(a) for the hexagonal-axis direction and in Fig. 8(b) for the hexagonal-plane direction. The magnetoresistance $[\rho(B) - \rho(0)]/\rho(0) = \Delta\rho/\rho$ is negative and reaches its maximum value at $T_C = 24$ K. The insets in Figs. 8(a) and 8(b) show the magnetoresistance at temperatures $T = 23$ and 2 K. For the hexagonal-axis direction, $\Delta\rho_6/\rho_6$ in a 9 T field amounts to –2.5% at 23 K and –1.0% at 2 K. For the hexagonal-plane direction, the magnetoresistance $\Delta\rho_p/\rho_p$ is approximately a factor of 2 smaller, amounting in 9 T to –1.5% at 23 K and –0.5% at 2 K.

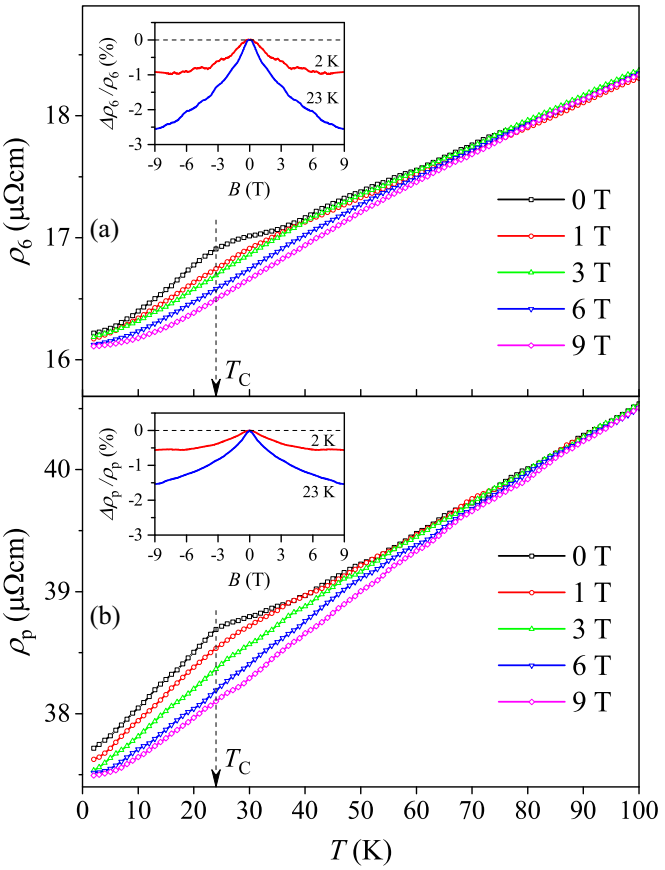

FIG. 8. Electrical resistivity in the temperature interval between 100 and 2 K, measured in magnetic fields between 0 and 9 T for (a) the hexagonal-axis direction (ρ_6) and (b) the hexagonal-plane direction (ρ_p). Dashed vertical line marks $T_C = 24$ K. Insets: magnetoresistance $\Delta\rho/\rho$ at temperatures $T = 23$ and 2 K.

C. Thermal conductivity

The thermal conductivity $\kappa(T)$ data measured along two orthogonal crystallographic directions (κ_6 and κ_p) are shown in Fig. 9. κ_6 and κ_p both increase rapidly in the low-temperature region up to about 40 K, whereas at higher temperatures the growth becomes slower and linearlike. Pronounced anisotropy between the hexagonal-axis and the hexagonal-plane directions is again observed, with $\kappa_6^{380\,\mathrm{K}} = 50\,\mathrm{W\,m^{-1}K^{-1}}$ and $\kappa_p^{380\,\mathrm{K}} = 24.5\,\mathrm{W\,m^{-1}K^{-1}}$. The thermal conductivity along the hexagonal-axis direction is thus a factor of 2 larger than along the hexagonal-plane direction, which is the same anisotropy as that observed in the electrical conductivity (the inverse electrical resistivity). No anomaly is observed at T_C.

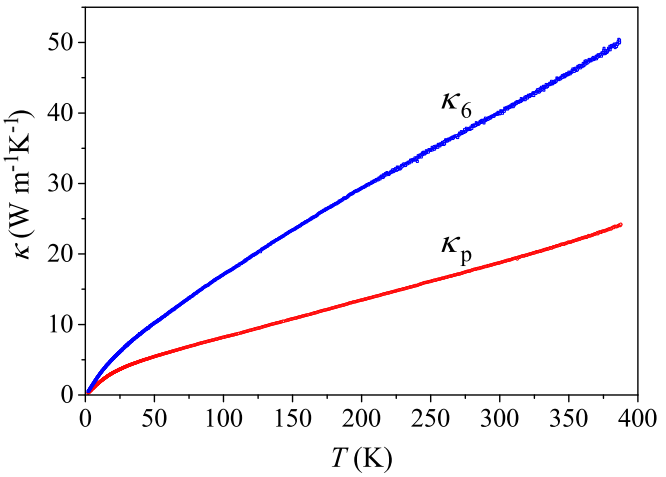

FIG. 9. Temperature-dependent thermal conductivity measured along the hexagonal-axis direction (κ_6) and in the hexagonal plane (κ_p).

D. Thermoelectric power

Thermoelectric power is sensitive to the sign of charge carriers and hence distinguishes between the negative electrons and the positive holes. The temperature-dependent thermopower [the Seebeck coefficient $S(T)$] between 2 and 380 K, measured along the hexagonal-axis direction (S_6) and in the hexagonal plane (S_p), is shown in Fig. 10. For both directions, the thermopower is positive and linearlike up to the highest investigated temperature. It shows pronounced anisotropy between the hexagonal-axis and the hexagonal-plane directions with $S_6^{380\,\mathrm{K}} = 8\,\mu\mathrm{V\,K^{-1}}$ and $S_p^{380\mathrm{K}} = 3.5\,\mu\mathrm{V\,K^{-1}}$. The thermopower along the hexagonal-axis direction is thus a factor of about 2 larger than that along the hexagonal-plane direction, and the thermopower values are typical metallic. Like the thermal conductivity, the thermopower also does not show any anomaly at T_C.

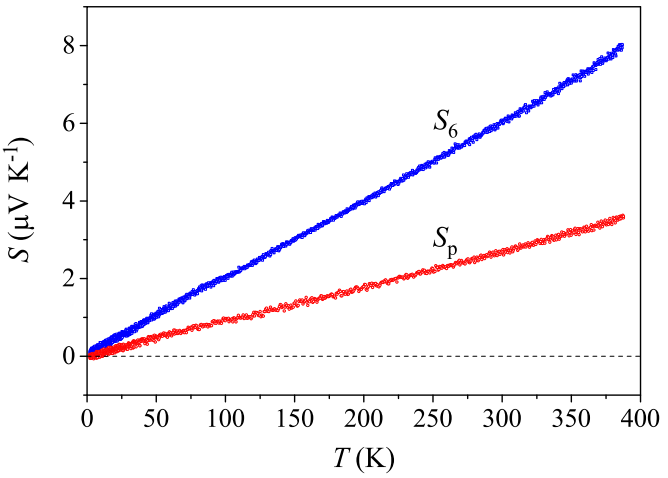

FIG. 10. Temperature-dependent thermoelectric power (the Seebeck coefficient), measured along the hexagonal-axis direction (S_6) and in the hexagonal plane (S_p).

E. Hall coefficient

The Hall coefficient is another quantity that distinguishes between electrons and holes. In magnetic metals, the Hall effect is decomposed into the normal Hall effect due to the Lorentz force acting on the conducting electrons in an external magnetic field and the anomalous Hall effect arising from the magnetization of the sample [18]. The two effects can be resolved from the measurement of Hall resistivity ρ_H, defined as the ratio of the transverse (Hall) electric field E_y over the current density j_x, when measured in a magnetic field B_z (here x, y, z Cartesian axes define the laboratory frame). The Hall resistivity is written as [19]

$$\rho_H = \frac{E_y}{j_x} = R_0 B_z + R_s \mu_0 M_z, \tag{2}$$

where R_0 is the normal Hall coefficient, R_s is the anomalous Hall coefficient, and M_z is the volume magnetization (in units $\mathrm{A\,m^{-1}}$), which is usually strongly temperature dependent. By measuring the $\rho_H(B)$ curves and knowing the $M(H)$ relation from independent measurements, R_0 and R_s can be resolved in the magnetically ordered phase. In the paramagnetic phase, the magnetization is linear in the magnetic field (obeying the Curie or Curie-Weiss law) so that the normal and anomalous terms of ρ_H exhibit the same dependence on B and cannot be resolved.

The Hall coefficient depends on the directions of the current (j_x), the Hall electric field (E_y), and the magnetic field (B_z) with respect to the crystallographic axes. The geometry of our sample allowed us to determine R_0 and R_s for one set of crystallographic directions. Magnetic field was directed along the hexagonal-plane [100] direction; the current was fed along the [001] hexagonal-axis direction, and the Hall field was perpendicular to these two directions (thus also lying in the hexagonal plane). The $M(H)$ curves shown in Fig. 5(b) (recalculated in the volume magnetization units) were used for the analysis, which was performed in the temperature range 2–50 K, where the $M(H)$ relation is nonlinear. A typical $\rho_H(B)$ curve, obtained at $T = 20\,\mathrm{K}$ for the magnetic field sweep ±9 T, is shown in Fig. 11(a). A fit with Eq. (2) (solid curve) has yielded the normal Hall coefficient $R_0 = -0.55 \times 10^{-10}\,\mathrm{m^3\,C^{-1}}$ and the anomalous Hall coefficient $R_s = -50 \times 10^{-10}\,\mathrm{m^3\,C^{-1}}$. The R_0 value is typical metallic, yielding the charge carrier density $n = 1.1 \times 10^{23}\,\mathrm{cm^{-3}}$, whereas its negative sign suggests that electrons are the majority charge carriers. The anomalous coefficient R_s is two orders of magnitude larger ($R_s/R_0 = 91$), a quite common situation in magnetic metals. The normal and anomalous contributions to ρ_H are also shown separately in Fig. 11(a). The temperature-dependent R_0 and R_s parameters are shown in Fig. 11(b), where it is observed that they do not show any pronounced variation with the temperature.

Opposed signs of the thermopower (its positive sign suggests that holes are the majority charge carriers) and the normal Hall coefficient (its negative sign suggests that electrons are the majority charge carriers) found in the $Cu_{84}Gd_9Ca_7$ crystal are not uncommon in intermetallic compounds. Such situations were reported, e.g., in high-T_C superconductors [20], the Y-phase Al-Co-Ni decagonal approximant [21], and the GaPd intermetallic phase [22]. At low temperatures, the temperature

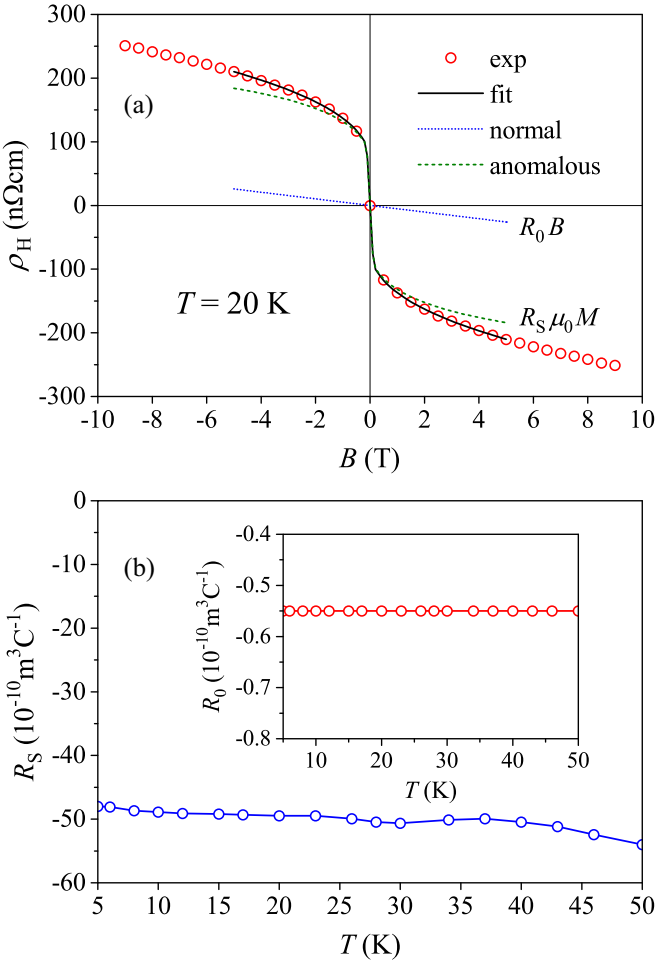

FIG. 11. (a) Hall resistivity $\rho_H(B)$ curve at $T = 20$ K. Solid curve is the fit with Eq. (2). The normal term $R_0 B$ and the anomalous term $R_s \mu_0 M$ of the Hall resistivity are also shown separately. (b) The anomalous Hall coefficient R_s in the temperature range 2–50 K. Inset: normal Hall coefficient R_0 in the same temperature range.

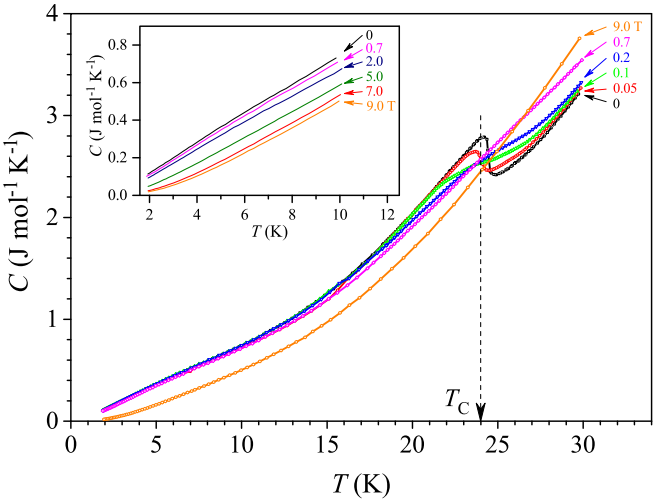

FIG. 12. Specific heat as a function of temperature in the interval from 2 to 30 K shown for a selected set of magnetic fields between 0 and 9 T. Dashed vertical line marks the zero-field transition temperature $T_C = 24$ K. Inset: magnetic-field dependence of the specific heat within the collective magnetic state in the low-temperature limit below 10 K.

dependence of the thermopower can be described by Mott's expression $S(T) = (\pi^2 k_B^2/3e)(d\ln\sigma(\varepsilon)/d\varepsilon)_{\varepsilon_F} T$, where e is the charge, $\sigma(\varepsilon)$ is the spectral conductivity function, and ε_F is the Fermi energy. Spectral conductivity is related to the electronic density of states (DOS) $g(\varepsilon)$ via the Einstein relation $\sigma(\varepsilon) = (e^2/V)g(\varepsilon)D(\varepsilon)$, where $D(\varepsilon)$ is the electronic spectral diffusivity and V is the sample volume. Under the assumption that the energy dependence of the spectral diffusivity can be neglected in the vicinity of the Fermi level, $D(\varepsilon) \approx D(\varepsilon_F)$, the quantity $d\ln\sigma(\varepsilon)/d\varepsilon$ can be replaced by $d\ln g(\varepsilon)/d\varepsilon$. The sign of the thermopower is consequently determined by two factors, the sign of the electric charge e and the sign of the DOS derivative at the Fermi energy $(dg(\varepsilon)/d\varepsilon)_{\varepsilon_F}$, so that the sign of the thermopower itself does not specify the sign of the charge carriers, like it does in free-electron metals [where $(dg(\varepsilon)/d\varepsilon)_{\varepsilon_F}$ is always positive]. In order to have consistent explanation of the signs of the Hall coefficient and the thermopower of $Cu_{84}Gd_9Ca_7$, and assuming that the negative sign of the normal Hall coefficient suggests electrons to be the majority charge carriers, positive thermopower would require negative value of the DOS derivative at the Fermi energy, $(dg(\varepsilon)/d\varepsilon)_{\varepsilon_F} < 0$. This hypothesis can be verified once the electronic DOS in the vicinity of ε_F will be known either experimentally or from a theoretical calculation.

F. Specific heat

Specific heat is another convenient quantity to characterize magnetic phase transitions. The specific heat of $Cu_{84}Gd_9Ca_7$ in the temperature interval from 2 to 30 K in magnetic fields between 0 and 9 T is shown in Fig. 12. A rather sharp anomaly (a jump), characteristic of a cooperative second-order phase transition, is observed in zero field at $T_C = 24$ K. The anomaly is gradually destroyed by the magnetic field already for small field values; while it is still observed in the fields of $B = 0.05$ and 0.1 T, it can no longer be detected at higher fields. The external magnetic field $B > 0.1$ T thus destroys the magnetically ordered spin structure that appears at T_C in zero field. Increasing magnetic field monotonously reduces the specific heat values in the temperature range below T_C, whereas for $T > T_C$ the in-field curves lie above the zero-field curve. Such behavior is typical for a collective magnetic state, where the external magnetic field "holds" the spins via the Zeeman interaction and impedes thermally induced spin fluctuations, which are then shifted to higher temperatures where $k_B T$ is larger than the sum of the exchange and the Zeeman interactions. The specific heat curves below 10 K are shown on an expanded scale in the inset of Fig. 12, where gradual reduction of the specific heat by the increasing magnetic field within the collective magnetic state is more evident, demonstrating that the magnetic part of the total specific heat is responsible for this effect.

The total specific heat C of a magnetic alloy is a sum of the electronic term $C_{\rm el}$, the lattice term $C_{\rm latt}$, and the magnetic term C_m [23]. The electronic term $C_{\rm el} = \gamma T$, where $\gamma = (\pi^2/3)k_B^2 g(\varepsilon_F)$, depends on the electronic DOS $g(\varepsilon_F)$ at the Fermi energy ε_F. In order to analyze the magnetic order in

the alloy, one needs to isolate the magnetic specific heat C_m from the total specific heat. This is possible when a suitable host exists, i.e., a nonmagnetic substance having similar electronic and crystal structures. The difference $C_{\text{alloy}} - C_{\text{host}}$ then gives the magnetic specific heat of the alloy. Regarding similarity of the crystal structures, which assures similar C_{latt} contributions, the Cu_5Ca compound seems to be a candidate for the host compound. However, the electronic specific heat coefficient γ of an alloy generally changes quite drastically when a rare-earth element is introduced due to a change of the DOS at ε_F, so that subtraction of the Cu_5Ca specific heat from that of the $Cu_{84}Gd_9Ca_7$ is not a valid procedure to isolate the magnetic specific heat of the latter. For that reason, quantitative analysis of the magnetic specific heat of $Cu_{84}Gd_9Ca_7$ could not be performed.

IV. DISCUSSION

The above-presented experimental results can be summarized as follows.

(i) Magnetic Gd atoms in the $Cu_{84}Gd_9Ca_7$ structure are located at the vertices of a hexagonal lattice, where they are randomly substituted by nonmagnetic Ca atoms. Magnetic lattice is thus disordered. Our crystal composition implies that the average occupancy of the mixed Gd/Ca site is slightly Gd rich. The distance between two nearest-neighbor Gd atoms is shorter along the hexagonal c axis ($r_{\text{Gd-Gd}} = c \approx 4.1$ Å) than in the hexagonal plane ($r_{\text{Gd-Gd}} = a \approx 5.1$ Å). At the unit cell edges along the hexagonal axis, there are two partially occupied copper Cu3 sites located between two Gd sites, with the Cu3 site occupation being rather low (about 6%). The intrinsic disorder in the $Cu_{84}Gd_9Ca_7$ unit cell originates from the substitutional disorder at the Gd/Ca site and the partial occupation of the Cu3 site.

(ii) Paramagnetic susceptibility demonstrates that the Gd magnetic moments assume their full free-ion values of μ_B, whereas the positive Curie-Weiss temperature reveals a FM-type parallel exchange coupling between the spins. Due to sizeable Gd moments, the magnetic dipole-dipole interaction is also significant.

(iii) Temperature-dependent dc magnetization in low magnetic fields shows a phase transition to a collective magnetic state at $T_C = 24$ K. In the lowest investigated magnetic field of $B = 0.5$ mT, M_{zfc} and M_{fc} are small, and their temperature variation is nontrivial, depending on the measurement protocol (different results were obtained for the fc measurement on cooling, fc measurement on heating, and zfc measurement on heating). In increasing magnetic fields, M_{zfc} and M_{fc} grow strongly up to some field value ($B \approx 0.1$ T for the field along the hexagonal-axis direction and $B \approx 0.4$ T for the field in the hexagonal plane), and the $M_{\text{zfc}} - M_{\text{fc}}$ difference decreases. For higher fields, the $M_{\text{zfc}} - M_{\text{fc}}$ difference vanishes, and the magnetization does not increase significantly with the magnetic field anymore. The growing external magnetic field smears the phase transition in the region of T_C over an increasingly larger temperature interval. For the field along the hexagonal-axis direction, the $M(T)$ curves resemble FM curves with a field-induced smearing of the phase transition, whereas for the field in the hexagonal plane, the low-field $M(T)$ curves resemble AFM curves and the increasing magnetic field gradually transforms the AFM-type temperature dependence into the FM-type.

Within the low-field region, the dc magnetization shows strong anisotropy between the hexagonal-axis direction and the hexagonal plane, whereas in higher magnetic fields the anisotropy vanishes.

(iv) The $M(H)$ curves also show strong anisotropy in the low-field region at temperature $T < T_C$. The system of Gd spins is easily polarizable along the hexagonal-axis direction, where a field as small as 20 mT is already enough to almost completely polarize the spins in the $T \to 0$ limit. For the field in the hexagonal plane, a significantly larger field of 400 mT is needed to achieve the same polarization. The hexagonal-axis direction can thus be considered as the easy axis of magnetization. The robustness of the magnetization anisotropy in the low-field regime is confirmed by the reproducible angular dependence of the magnetization for rotation about an axis lying in the hexagonal plane.

The $M(H)$ hysteresis loops are also anisotropic, showing a very small coercive field for the hexagonal-axis direction and zero coercive field for the hexagonal-plane direction of the magnetic field. The $Cu_{84}Gd_9Ca_7$ is thus a magnetically soft material.

(v) Ac susceptibility measurements were performed by using the ac field of amplitude 0.65 mT, which was small enough that the internal magnetic structure below T_C was not perturbed significantly by the field. For the ac field applied along the hexagonal axis, the real part of the ac susceptibility χ' develops a sharp peak at T_C, whose very weak frequency dependence suggests a thermodynamic phase transition, but there is a narrow superparamagnetic regime in the vicinity of T_C where spins (or spin clusters) perform thermally assisted jumping between energetically similar states and gradually freeze below T_C. In the low-temperature region below about 20 K, χ' develops a broad maximum, which is produced by spin fluctuations representing the elementary excitations of the collective magnetic state that develops below T_C. When the ac field is applied in the hexagonal plane, the spins system is considerably stiffer, and the spin entities are less reorientable by the external magnetic force.

(vi) The TRM decay experiments show that ergodicity of the spin system is broken on the experimental time scale in the collective magnetic state below T_C, indicating that frustration of magnetic interactions between the Gd spins is present. The TRM decays are logarithmically slow in time, and within the investigated time interval of 120 min it cannot be concluded to what kind of equilibrium state the spin system approaches in the $t \to \infty$ limit (either to a state with nonzero spontaneous magnetization or to a zero-magnetization state).

(vii) The question whether the zero-field equilibrium state possesses zero- or nonzero spontaneous magnetization can also not be satisfactorily answered from the dc magnetization measurements. M_{zfc} and M_{fc} in the lowest investigated magnetic field of $B = 0.5$ mT are both very small but different from zero, and the magnetization values for the field along the hexagonal-axis direction are by a factor of about 5 larger than for the hexagonal-plane direction. Since the spin system can be polarized already by a tiny magnetic field and the polarization is much easier along the hexagonal-axis direction,

this suggests that M_{zfc} and M_{fc} in this small magnetic field could already be affected significantly by the field. If the spontaneous magnetization exists, it is very small.

(viii) Electrical resistivity in zero magnetic field shows an enhancement with respect to the resistivity in a high magnetic field (such as 9 T) at temperatures below about 70 K, and the enhancement reaches its maximum at T_C. This enhancement results in a negative magnetoresistance. Increasing magnetic field gradually destroys the resistivity enhancement, demonstrating that it originates from a magnetic contribution to the electrical resistivity. The underlying mechanism is the exchange interaction between the conduction electrons and the Gd 4f electrons, where the fluctuating Gd moments induce conduction-electron transitions from an occupied state $|\vec{k}\sigma\rangle$ to an unoccupied state $|\vec{k}'\sigma'\rangle$, where $\vec{k}$ is the wave vector and σ the spin variable of the conduction electron. Increasing magnetic field impedes Gd spin fluctuations, which in turn decreases the magnetic contribution to the electrical resistivity. The fact that the magnetic enhancement of the electrical resistivity is observed already much above T_C (at about 70 K) and that the enhancement reaches its maximum at T_C shows that short-range-ordered clusters of Gd moments start to form much above the phase transition and the cluster fluctuations are most intense at T_C, in agreement with the ac susceptibility that shows a superparamagnetic regime of rapidly reorienting spin clusters in the vicinity of T_C.

(ix) The zero-field specific heat shows an anomaly (a jump) at T_C, characteristic of a cooperative second-order phase transition. The anomaly is gradually destroyed by the magnetic field and could not be detected anymore in fields $B > 0.1$ T. External magnetic field destroys the magnetically ordered spin structure that appears at T_C in zero and low fields. Increasing magnetic field monotonously reduces the specific heat values in the temperature range below T_C, demonstrating that the magnetic part of the total specific heat is responsible for this effect. Such behavior is typical for a collective magnetic state, where the external magnetic field holds the spins via the Zeeman interaction and impedes thermally induced spin fluctuations, which contribute increasingly less to the magnetic specific heat.

(x) The electrical and thermal conductivities and the thermoelectric power are anisotropic, all being a factor of about 2 larger along the hexagonal-axis direction as compared to the hexagonal-plane direction. This is very likely a consequence of shorter interatomic distances along the hexagonal c axis in the unit cell, which makes the electronic and heat transport easier in that direction.

The above results suggest the following model of magnetism in the $Cu_{84}Gd_9Ca_7$ crystal. The collective magnetic state below T_C achieved in zero and low magnetic fields originates from interacting Gd moments, occupying the mixed Gd/Ca site in the hexagonal lattice. The interaction responsible for magnetic ordering is the conduction-electrons-mediated indirect exchange, which is a spatially isotropic interaction and does not specify any orientation of the moments relative to the crystal axes. The moments' directions in the crystal lattice are fixed by the magnetic anisotropy, which is present in addition to the exchange. For the rare-earth ions in a solid environment, the dominant source of anisotropy is usually the electrostatic interaction of the anisotropic $4f$ charge cloud with the crystalline electric fields. Gadolinium is, however, an exception because Gd^{3+} is an S-state ion with a spherically symmetric $4f$ charge cloud (its orbital angular momentum is zero, $L = 0$) so that the crystal-field interaction vanishes. A much smaller magnetic anisotropy is in this case produced by the dipole–dipole coupling between the Gd moments, which is both highly anisotropic and extremely long-ranged interaction. It is known that in the pure gadolinium hexagonal close-packed metal, dipolar anisotropy is responsible for the moments' orientation along the hexagonal c axis just below the transition to the FM phase [24,25]. Magnetic Hamiltonian of the system of interacting Gd ions, possessing an angular momentum $\vec{J}$ and a magnetic moment $\vec{\mu} = -g\mu_B\vec{J}$ in an external magnetic field $\vec{B}$ can be written as [26]

$$\mathcal{H} = -\frac{1}{2}\sum_{i\neq j} c_i c_j \mathcal{J}(ij)\vec{J}_i\cdot\vec{J}_j - \frac{1}{2}\sum_{i\neq j} c_i c_j \sum_{\alpha,\beta}\Delta\mathcal{J}_{\alpha\beta}(ij)J_{i\alpha}J_{j\beta} + g\mu_B\sum_i c_i\vec{J}_i\cdot\vec{B}. \tag{3}$$

The first term on the right of Eq. (3) is the isotropic indirect exchange, which in the case of $Cu_{84}Gd_9Ca_7$, favors FM exchange ($\mathcal{J}(ij) > 0$). The summation runs over all mixed Gd/Ca sites of the hexagonal lattice, and the random Gd-for-Ca substitution is taken into account by the variable c_i, which is 1 if the ion on site i is Gd and 0 if the site is occupied by Ca. The configurational average $\langle c_i\rangle_{cf} = c$ then yields the atomic concentration of Gd in the crystal. The second term is the classical magnetic dipole–dipole interaction between a pair of moments $\vec{\mu}_i$ and $\vec{\mu}_j$ located at the lattice sites $\vec{R}_i$ and $\vec{R}_j$. The summation indices α,β run over x,y,z, and the coupling parameter $\Delta\mathcal{J}_{\alpha\beta}(ij)$ is expressed as

$$\Delta\mathcal{J}_{\alpha\beta}(ij) = (\mu_0/4\pi)(g\mu_B)^2 \times \frac{3(R_{i\alpha}-R_{j\alpha})(R_{i\beta}-R_{j\beta}) - \delta_{\alpha\beta}|\vec{R}_i-\vec{R}_j|^2}{|\vec{R}_i-\vec{R}_j|^5}. \tag{4}$$

The last term is the Zeeman interaction between the moments $\vec{\mu}_i$ and the external magnetic field $\vec{B}$. The main problem in solving the disordered Hamiltonian of Eq. (3) and in determining theoretically the magnetic field–temperature phase diagram is the random positioning of Gd moments at a particular site of the hexagonal lattice, where all Gd moments in the crystal interact and participate in the collective magnetic state. Some qualitative conclusions can nevertheless be drawn.

The exchange coupling favors FM ordering of the Gd moments at low temperatures. Since in our crystal the Gd concentration is slightly higher than that of Ca, Gd spins are abundant in the lattice and a bit more than half of the mixed Gd/Ca sites are occupied by a spin. It is likely that some chemical clustering in the form of Gd-rich and Gd-poor domains occurs, where the domains vary in size and are randomly distributed over the crystal. It should be mentioned that x-ray spectra did not exhibit any superstructure peaks due to chemical ordering between Gd and Ca, so that there is no direct indication of clustering from XRD.

Gd-rich domains (conveniently termed as spin clusters) are very likely small spin entities, where the local coordination of a given Gd atom contains more Gd neighbors than the average composition. Based on our experiments (the zero-field specific heat exhibits a rather sharp peak at T_C and the magnetization in the lowest investigated field of $B = 0.5$ mT shows a sharp increase at the phase transition), it is reasonable to consider that the FM exchange coupling strength is rather uniform over the crystal so that the disorder-induced distribution of the coupling constants is narrow. Magnetic anisotropy produced by the long-ranged dipolar interaction between randomly distributed Gd spins varies in space at the local level, and the distribution of the anisotropy fields can be considered as random. The Gd spin system in the $Cu_{84}Gd_9Ca_7$ crystal can thus be, to a fair approximation, modeled as a system of spins possessing uniform FM exchange interactions and random anisotropies. Upon cooling the crystal in zero magnetic field (or in a field much smaller than the dipolar anisotropy fields) from the paramagnetic phase, the spins order ferromagnetically at the Curie temperature $T_C = 24$ K, but the distribution of anisotropies implies that the magnetic structure breaks into differently oriented FM domains. High degeneracy of spin configurations in the phase space is reflected in an irreversible behavior of the temperature-dependent zfc and fc magnetizations below T_C, where different configurations are achieved for different thermal histories (fc measurement on cooling, fc measurement on heating, and zfc measurement on heating), as shown in the insets of Figs. 2(a) and (b). The zero-field collective magnetic state of $Cu_{84}Gd_9Ca_7$ can thus be described as a FM state with random anisotropies.

By applying the external magnetic field, the Zeeman interaction starts to compete with the dipolar anisotropy in determining spin orientations. The spins are easily polarizable along the hexagonal axis, whereas a significantly stronger field is needed to reorient the spins from the hexagonal direction into the hexagonal plane. Increasing magnetic field drives the temperature dependence of the magnetization at $T < T_C$ towards that of a site-ordered ferromagnet with $M \propto (T_C - T)^{\beta}$ (where $\beta \approx 1/2$). This indicates that the Zeeman interaction starts to dominate over the random-dipolar anisotropy already at small fields and coerces the FM domains into alignment along the external field direction. At the same time, external magnetic field smears the FM phase transition.

The narrow superparamagnetic regime in the close vicinity of T_C, best observed in the ac susceptibility, can be understood by assuming thermally reorienting Gd spin clusters. In the region of T_C, cluster magnetic moments are still very small so that clusters can be considered to a good approximation as noninteracting and their moments can rotate almost freely in the local dipolar fields (which are also small due thermal reorientations of the Gd spins that produce the anisotropy fields). Upon cooling below T_C, the cluster moments, the inter-cluster interactions, and the dipolar anisotropy fields all rapidly increase and impede thermally induced cluster reorientations, which terminates the superparamagnetic regime.

The growth of the dipolar anisotropy fields upon the spin-cluster reorientations freeze-out below T_C also explains the transformation of the FM-type temperature dependence of M_{zfc} and M_{fc} into the AFM-type, observed during cooling in a fixed (low) magnetic field applied in the hexagonal plane [Fig. 2(b)]. Just below T_C, rapidly reorienting spin clusters produce small time-average anisotropy fields so that already a small external magnetic field is able to polarize the FM domains into the field direction. The temperature dependence of M_{zfc} and M_{fc} is consequently that of a field-induced FM. Upon lowering the temperature, the spin-cluster reorientations slow down, and the random-anisotropy fields grow and win over the external magnetic field at a particular temperature [marked by a solid vertical arrow in Fig. 2(b)]. At that temperature, the magnetic structure of aligned FM domains breaks into a structure of differently oriented FM domains, which reduces the total magnetization, and the temperature dependence of M_{zfc} and M_{fc} becomes AFM-like.

It is interesting to consider the relation of the random-anisotropy FM state observed in the $Cu_{84}Gd_9Ca_7$ to a spin-glass state. According to a standard definition [27,28], a system is classified as a spin glass when it possesses two fundamental properties: (a) frustration and (b) randomness (the spins must be positioned randomly in the sample). If random anisotropies are present, even a system with uniform exchange interactions possesses the two ingredients of randomness and frustration that are necessary for spin-glass behavior [29,30]. Similarly to spin glasses, competition between the exchange and the random anisotropies gives rise to many degenerate minima in the phase space. Cooling the spin system with uniform FM exchange interactions in random-anisotropy fields creates FM domains at low temperatures, which are trapped in different orientations. The distribution of domain orientations depends on the cooling rate and the presence or absence of even a minute magnetic field. Such a state is metastable, and the nonergodic spin system will relax slowly towards some equilibrium state, which may either possess nonzero spontaneous magnetization or no net magnetization. Due to macroscopic equilibration times, these two possibilities are difficult to discriminate experimentally. The random-anisotropy system will thus exhibit spin-glasslike characteristics in the dynamics (slowly decaying metastable states, ultraslow dynamics of the thermoremanent magnetization, etc.) [31–33]. The random-anisotropy FM state observed in the $Cu_{84}Gd_9Ca_7$ belongs to the class of disordered ferromagnets, which may be considered as a subclass of the generic class of spin glasses. The spin-glass behavior originating from the inherent disorder in the crystal lattice is quite commonly found in intrinsically disordered complex intermetallics containing transition metals and rare-earth elements. Examples are the *i*-Tb-Mg-Zn(Cd) icosahedral quasicrystals [34–40] and the giant-unit-cell complex metallic alloys T-Al_3Mn [41], μ-Al_4Mn [42], and $Gd_3Au_{13}Sn_4$ [43]. The main difference between the $Cu_{84}Gd_9Ca_7$ and the above-mentioned intrinsically disordered complex intermetallics is the type of interspin interactions. In the latter systems, the interactions are in all cases AFM, favoring antiparallel spin ordering, so that these systems can be considered to belong to the subclass of strongly disordered antiferromagnets within the generic class of spin glasses.

V. CONCLUSIONS

By applying the alloy design concept that stable intermetallic phases between two 100% immiscible elements

can be formed by adding a third element that forms stable compounds with both elements, we have explored the ternary Cu–Gd–Ca phase diagram in its Cu-rich corner along the $Cu_5Gd_{1-x}Ca_x$ composition line, where copper acts as the mediating element between the immiscible Gd and Ca. We have successfully synthesized a compound with the average composition $Cu_{84}Gd_9Ca_7$ (equivalent to $Cu_5Gd_{0.54}Ca_{0.42}$), which is the first known stable intermetallic compound of Cu, Gd, and Ca. This opens the possibility to search for new ternary intermetallic phases in the Cu–Gd–Ca phase diagram, including giant-unit-cell structurally complex phases and quasicrystals. It is reasonable to expect that such phases may exist in the region of the phase diagram with high concentration of the mediating element, hence in the Cu-rich corner, whereas the existence of intermetallic compounds in the Cu-poor part of the phase diagram may remain unknown forever. The random substitution of magnetic Gd by nonmagnetic Ca atoms at the mixed Gd/Ca site in the hexagonal unit cell makes the magnetic Gd lattice disordered, which leads to interesting magnetic ordering at low temperatures that occurs at $T_C = 24$ K in zero and low external magnetic fields. The zero-field collective magnetic state can be described as a random-anisotropy FM state, where random magnetic anisotropies originate from the magnetic dipole interactions between the Gd moments in the magnetically disordered lattice. The random-anisotropy FM state in the $Cu_{84}Gd_9Ca_7$ is characterized by randomness and frustration of magnetic interactions, which are the two ingredients that allow classifying this state into the generic class of spin glasses and into its subclass of disordered ferromagnets. Such systems are rare among the intrinsically disordered complex intermetallics.

ACKNOWLEDGMENTS

The present paper was financed in part by a French-Slovene collaboration established under Push-Pull Alloys and Complex Compounds (PACS2) Joint Open Laboratory. We are grateful to CNRS, Université de Lorraine and Slovenian Research Agency for the provision of funding.

[1] K. A. Gschneidner and F. W. Calderwood, Bull. Alloy Phase Diag. **8**, 515 (1987).
[2] D. Gratias, Y. Calvayrac, J. Devaud-Rzepski, F. Faudot, M. Harmelin, A. Quivy, and P. A. Bancel, J. Non-Cryst. Solids **153–154**, 482 (1993).
[3] T. Weber, J. Dshemuchadse, M. Kobas, M. Conrad, B. Harbrecht, and W. Steurer, Acta, Cryst. B **65**, 308 (2009).
[4] G. Bruzzone, J. Less-Common Met. **25**, 361 (1971).
[5] D. J. Chakrabarti and D. E. Laughlin, Bull. Alloy Phase Diag. **5**, 570 (1984).
[6] J. H. Wernick and S. Geller, Acta Cryst. **12**, 662 (1959).
[7] K. H. J. Buschow, A. S. Van Der Goot, and J. Birkhan, J. Less-Common Met. **19**, 433 (1969).
[8] K. H. J. Buschow, and A. S. Van Der Goot, Acta Cryst. B **27**, 1085 (1971).
[9] M. M. Carnasciali, S. Cirafici, and E. Franceschi, J. Less-Common Met. **92**, 143 (1983).
[10] P. R. Subramanian and D. E. Laughlin, Bull. Alloy Phase Diag. **9**, 347 (1988).
[11] H. Okamoto, J. Phase Equil. Diff. **34**, 57 (2013).
[12] See Supplemental Material at http://link.aps.org/supplemental/10.1103/PhysRevB.93.094202 for details on the crystal synthesis, characterization, and structure determination.
[13] J. A. Mydosh, *Spin Glasses: An Experimental Introduction* (Taylor & Francis, London, 1993), p. 67.
[14] F. E. Mabbs and D. J. Machin, *Magnetism and Transition Metal Complexes* (Chapman and Hall, London, 1973), p. 7.
[15] See, e.g., N. W. Aschroft and N. D. Mermin, *Solid State Physics* (Saunders College Publishing, London, 1976), p. 711.
[16] M. Lederman, R. Orbach, J. M. Hammann, M. Ocio, and E. Vincent, Phys. Rev. B **44**, 7403 (1991).
[17] D. Chu, G. G. Kenning, and R. Orbach, Phil. Mag. B **71**, 479 (1995).
[18] C. M. Hurd, *The Hall Effect in Metals and Alloys* (Plenum, New York, 1972).
[19] See, e.g., U. Mizutani, *Introduction to the Electron Theory of Metals* (Cambridge University Press, Cambridge, 2001), p. 428.
[20] Y. Kubo, Phys. Rev. B **50**, 3181 (1994).
[21] A. Smontara, I. Smiljanić, J. Ivkov, D. Stanić, O. S. Barišić, Z. Jagličić, P. Gille, M. Komelj, P. Jeglič, M. Bobnar, and J. Dolinšek, Phys. Rev. B **78**, 104204 (2008).
[22] M. Klanjšek, A. Gradišek, A. Kocjan, M. Bobnar, P. Jeglič, M. Wencka, Z. Jagličić, P. Popčević, J. Ivkov, A. Smontara, P. Gille, M. Armbrüster, Yu. Grin, and J. Dolinšek, J. Phys.: Condens. Matter **24**, 085703 (2012).
[23] See, e.g., A. Tari, The Specific Heat of Matter at Low Temperatures (Imperial College Press, London, 2003).
[24] M. S. S. Brooks and D. A. Goodings, J. Phys. C **1**, 1279 (1968).
[25] W. D. Corner and B. K. Tanner, J. Phys. C **9**, 627 (1976).
[26] See, e.g., J. Jensen and A. R. Mackintosh, *Rare Earth Magnetism* (Clarendon Press, Oxford, 1991), Chap. 1.4.
[27] K. Binder and A. P. Young, Rev. Mod. Phys. **58**, 801 (1986).
[28] Edited by H. T. Diep, *Frustrated Spin Systems* (World Scientific, Singapore, 2004) and references therein.
[29] Y. Imry and S. Ma, Phys. Rev. Lett. **35**, 1399 (1975).
[30] R. Harris, M. Plischke, and M. J. Zuckermann, Phys. Rev. Lett. **31**, 160 (1973).
[31] J. Villain, Phys. Rev. Lett. **52**, 1543 (1984).
[32] G. Grinstein and J. F. Fernandez, Phys. Rev. B **29**, 6389 (1984).
[33] E. Pytte and J. F. Fernandez, Phys. Rev. B **31**, 616 (1985).
[34] I. R. Fisher, K. O. Cheon, A. F. Panchula, P. C. Canfield, M. Chernikov, H. R. Ott, and K. Dennis, Phys. Rev. B **59**, 308 (1999).
[35] J. Dolinšek, Z. Jagličić, M. A. Chernikov, I. R. Fisher, and P. C. Canfield, Phys. Rev. B **64**, 224209 (2001).
[36] T. J. Sato, J. Guo, and A. P. Tsai, J. Phys.: Condens. Matter **13**, L105 (2001).
[37] J. Dolinšek, Z. Jagličić, T. J. Sato, J. Q. Guo, and A. P. Tsai, J. Phys.: Condens. Matter **15**, 7981 (2003).
[38] S. E. Sebastian, T. Huie, I. R. Fisher, K. W. Dennis, and M. J. Kramer, Philos. Mag. **84**, 1029 (2004).

[39] T. J. Sato, H. Takakura, A. P. Tsai, and K. Shibata, Phys. Rev. Lett. **81**, 2364 (1998).

[40] T. J. Sato, H. Takakura, A. P. Tsai, K. Shibata, K. Ohoyama, and K. H. Andersen, Phys. Rev. B **61**, 476 (2000).

[41] J. Dolinšek, J. Slanovec, Z. Jagličić, M. Heggen, S. Balanetskyy, M. Feuerbacher, and K. Urban, Phys. Rev. B **77**, 064430 (2008).

[42] S. Jazbec, Z. Jagličić, S. Vrtnik, M. Wencka, M. Feuerbacher, M. Heggen, S. Roitsch, and J. Dolinšek, J. Phys.: Condens. Matter **23**, 045702 (2011).

[43] P. Koželj, S. Jazbec, S. Vrtnik, A. Jelen, J. Dolinšek, M. Jagodič, Z. Jagličić, P. Boulet, M. C. de Weerd, J. Ledieu, J. M. Dubois, and V. Fournée, Phys. Rev. B **88**, 214202 (2013).